

## Spatial ordering due to hydrodynamic interactions between a pair of colliding drops in a confined shear

Kausik Sarkar and Rajesh Kumar Singh

Citation: *Phys. Fluids* **25**, 051702 (2013); doi: 10.1063/1.4805082

View online: <http://dx.doi.org/10.1063/1.4805082>

View Table of Contents: <http://pof.aip.org/resource/1/PHFLE6/v25/i5>

Published by the [American Institute of Physics](#).

---

### Additional information on Phys. Fluids

Journal Homepage: <http://pof.aip.org/>

Journal Information: [http://pof.aip.org/about/about\\_the\\_journal](http://pof.aip.org/about/about_the_journal)

Top downloads: [http://pof.aip.org/features/most\\_downloaded](http://pof.aip.org/features/most_downloaded)

Information for Authors: <http://pof.aip.org/authors>

### ADVERTISEMENT



**Running in Circles Looking  
for the Best Science Job?**

Search hundreds of exciting  
new jobs each month!

<http://careers.physicstoday.org/jobs>

physicstodayJOBS



## Spatial ordering due to hydrodynamic interactions between a pair of colliding drops in a confined shear

Kausik Sarkar<sup>1,2,3</sup> and Rajesh Kumar Singh<sup>2,3</sup>

<sup>1</sup>*Department of Mechanical and Aerospace Engineering, George Washington University, Washington, DC 20052, USA*

<sup>2</sup>*Department of Mechanical Engineering, University of Delaware, Newark, Delaware 19716, USA*

<sup>3</sup>*Biomechanics and Movement Science Program, University of Delaware, Newark, Delaware 19716, USA*

(Received 5 January 2013; accepted 29 April 2013; published online 21 May 2013)

Pair-collision between viscous drops in a confined shear is simulated to show that the confinement alters the trajectories of the drops spatially ordering them at a finite separation in the center of the domain. In contrast to free shear where drops eventually adopt free streamlines with a finite cross-stream separation, here they move towards the centerline achieving zero cross-stream separation but a net stream-wise separation. The latter varies as inverse of capillary number and cube of the confinement (distance between the walls). The final stream-wise separation does not depend on the initial positions of the drops when the drops are in the same shear plane. The separation decreases approximately linearly with the initial separation in the vorticity direction. An analytical theory explaining the phenomenon is presented. Effects of the ratio of drop to matrix viscosity are briefly investigated. © 2013 AIP Publishing LLC. [<http://dx.doi.org/10.1063/1.4805082>]

Hydrodynamic interactions between deformable particles and the bounding walls in a confined shear are important in microfluidic applications<sup>1–4</sup> and microcirculatory flows.<sup>5</sup> Due to the small size and velocity, the flow is governed often by the inertia-less Stokes flow. Stokes flow is linear and therefore reversible. A number of counterintuitive phenomena are observed in particulate Stokes flows due to the flow reversibility.<sup>6</sup> For instance, in a free shear, a rigid sphere does not experience any cross-stream motion,<sup>7</sup> or a pair of rigid spheres continues in their original streamlines after collision maintaining the pre-collision cross-stream separation. However, for drops, the reversibility is broken; drops migrate away from a bounding wall,<sup>8,9</sup> and a colliding pair of drops in free shear increases their cross-stream separation leading to an enhanced shear induced particle diffusion in emulsions.<sup>10,11</sup> Reversibility is also broken in presence of finite inertia.<sup>12,13</sup> Finite inertia induces particle migration to an intermediate position (0.6 radial distance) in a Poiseuille flow first observed by Segre and Silberberg;<sup>14</sup> this inspired a series of theoretical and experimental efforts targeted at understanding the underlying physics of inertial migration.<sup>15–20</sup>

Recently, we showed that deformation and inertia can work in unison to generate a new type—reversed (type II)—of trajectories for a pair of drops in free shear not seen in Stokes flow.<sup>12,13</sup> Such reversed trajectories are also seen in presence of inertia for a pair of rigid spheres.<sup>21</sup> The underlying mechanism has been identified as the inertia induced reversed streamlines around a single sphere.<sup>22,23</sup> On the other hand, in the Stokes limit, in a confined shear a similar reversed (called swapping trajectory by the authors) trajectory for a pair of rigid spheres is discovered due to interactions with the bounding walls.<sup>24</sup> Reversibility leads to a swapping of pre-collision streamlines between spheres. Swapping trajectories have been proposed as a probable cause for experimentally observed anomalous particle diffusion.<sup>25</sup> Here, we show that in presence of both deformation and confinement, pair interaction gives rise to a specific spatial positioning of drops at fixed separation in the center of the confined domain.

We numerically simulate the collision of a pair of initially spherical drops of radius  $a$  in a confined shear bounded by walls oriented along the  $x$ -axis separated by a distance  $L_y$  using a front

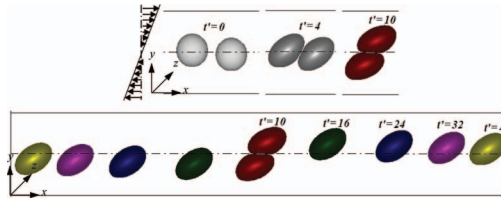


FIG. 1. Hydrodynamic interaction of a pair of drops in a confined shear for  $Ca = 0.2$ ,  $L_y = 5a$ ,  $\Delta x_0/a = 2.5$ , and  $\Delta y_0/a = 0.25$ . Drops travel towards the center of the domain.

tracking finite difference method.<sup>26–29</sup> The method has been used to study a number of different problems, including pair interactions in an unbounded shear. The code has been carefully validated by demonstrating excellent match with prior experimental observations.<sup>10,12</sup> Here the walls are moved with equal and opposite  $x$ -directional velocities to generate a shear  $\dot{\gamma}$ . The dynamics depends on the capillary number  $Ca = \mu_m \dot{\gamma} a / \Gamma$ , viscosity ratio ( $\lambda = \mu_d / \mu_m$ ), and degree of confinement  $L_y/a$ .  $\mu_m$  and  $\mu_d$  are matrix and drop phase viscosities, and  $\Gamma$  is the interfacial tension. Since the code is not fully implicit, we are limited to simulations with small but finite non-zero inertia. We consider  $Re (= \rho_m \dot{\gamma} a^2 / \mu_m) = 0.02$  as a surrogate for Stokes flow simulation.  $\rho_m$  is the density of the matrix phase. We use a computational domain  $L_x = 50a$  and  $L_z = 5a$ . Mostly we consider the case of drops initially placed in the same central  $z$ -plane; effects of separation in the vorticity direction have been briefly considered. We vary  $L_y$  to study the effects of confinement on the trajectory of the drops. In the flow ( $x$ ) and the vorticity ( $z$ ) directions periodic boundary conditions are used.

The drops driven by the imposed shear interact, deform—maximum deformation being when they press against each other along the compression axis of the imposed shear—then separate, and move in opposite directions (a typical case is shown in Figure 1). However, in contrast to free shear, here after collision drops do not eventually follow any free streamline.<sup>10,11</sup> Neither do they achieve a net cross-stream separation. Instead, drops experience a wall induced lateral migration that moves them to the center line, progressively reducing their cross-stream displacement to zero (Figure 2(a)). Finally, they achieve a state of relative equilibrium separated by an equilibrium distance  $\Delta x_{final}/a$  at the centerline. This is shown explicitly for the case of  $L_y/a = 4.5$  in Figure 2(b). For much larger  $L_y/a$ ,  $\Delta x_{final}/a$  becomes larger, and hence requires much longer simulation in far longer (larger  $L_x/a$ ) computational domain. However, after collision, the drop trajectory eventually becomes a straight line (as can be seen in Figure 2) and therefore,  $\Delta x_{final}/a$  can be determined by linear extrapolation. The validity of this extrapolation procedure has been carefully examined and established for several  $L_y/a$  by using simulations in longer domains. Only in the limit of very large inter-wall separation ( $L_y/a \sim 20$ ), wall effects are negligible.

In Figure 3, we investigate the effects of initial separation on the drop trajectory. Changing initial separation changes trajectory type—increasing initial stream-wise or decreasing initial cross-stream separation leads to reversed or swapping (type II) trajectory both for rigid spheres and drops.<sup>12</sup> However, here we consider those initial positions which do not change the trajectory type. With this restriction, Figure 3 shows that  $\Delta x_{final}/a$  remains independent of initial positions when

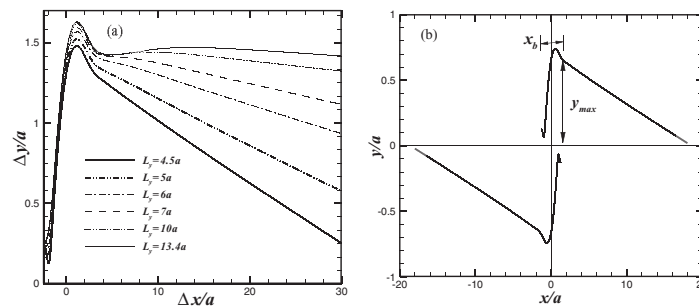


FIG. 2. (a) Relative trajectory of the drops at  $Ca = 0.2$ ,  $\Delta x_0/a = 2.5$ , and  $\Delta y_0/a = 0.25$  for different  $L_y$  values. (b) The actual trajectories in the domain  $L_y = 4.5a$ .

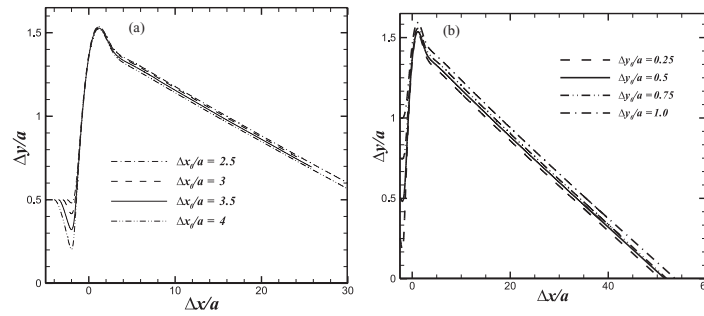


FIG. 3. Effects of the initial positions on the relative trajectory: (a) Variation of initial separation in the flow direction  $\Delta x_0/a$  for  $\Delta y_0/a = 0.50$ ,  $Ca = 0.20$ , and  $L_y = 5a$ . (b) Effects of initial separation in the gradient direction  $\Delta y_0/a$  for  $\Delta x_0/a = 2.50$  in the same domain and for the same capillary number.

the drops are in the same shear plane. In Figure 4(a), we consider the effect of initial separation in the vorticity direction ( $\Delta z_0/a \neq 0$ ). For  $\Delta z_0/a \geq 0.75$ , drops follow reversed trajectories. One obtains passing trajectories for smaller  $\Delta z_0/a$ ; in this range as  $\Delta z_0/a$  is increased,  $\Delta x_{final}/a$  decreases approximately linearly (Figure 4(b)). However, unlike when drops are in the same shear plane (Figure 3), for  $\Delta z_0/a \neq 0$ ,  $\Delta x_{final}/a$  does not remain completely independent of  $\Delta x_0/a$  and  $\Delta y_0/a$  (not shown here for brevity). Henceforth, we choose drops in the same shear plane and initial separation in the flow and the gradient directions fixed at  $\Delta x_0/a = 2.5$  and  $\Delta y_0/a = 0.25$ .

In Figure 5(a), we show that trajectories for different  $L_y/a$  (from simulations in Figure 2) result in  $\Delta x_{final}/a \sim (L_y/a)^3$  for  $Ca = 0.2$ . By varying capillary number for three different confinements, we obtain  $\Delta x_{final}/a \sim 1/Ca$  shown in Figure 5(b). For  $Ca > 0.35$ , drops experience large stretching and possible breakup—confinement is known to delay breakup.<sup>30</sup> They are not considered here.

In the following, we explain quantitatively the main result—numerically observed scaling for the stream-wise separation:

$$\frac{\Delta x_{final}}{a} \sim \frac{1}{Ca} \left( \frac{L_y}{a} \right)^3. \quad (1)$$

We show that the result stems primarily from drops being driven by wall induced migration. Although the process cannot take place without drop-collision, the interactions between drops do not play any role long time after collision. We first note that the drop trajectories after collision, as shown above, are approximately straight lines (Figure 2). That forces attention on the drop velocity. In the flow direction the velocity of the drop post-collision is dominated by the imposed shear and therefore can be approximated as  $u_x = \dot{\gamma} y$ , neglecting the small slip velocity as well as the effect due to the interaction with the other drop, the result becomes more accurate as the drop approaches the centerline. In Figure 6(a), we note that the lateral velocity  $u_y \sim -y$  especially near the centerline after the effects of collision decays. This explains the straight line trajectory of the drop after collision:  $dx/dy = u_x/u_y \approx \text{constant}$ . Furthermore, by appropriately rescaling the variables, Figure 6(b)

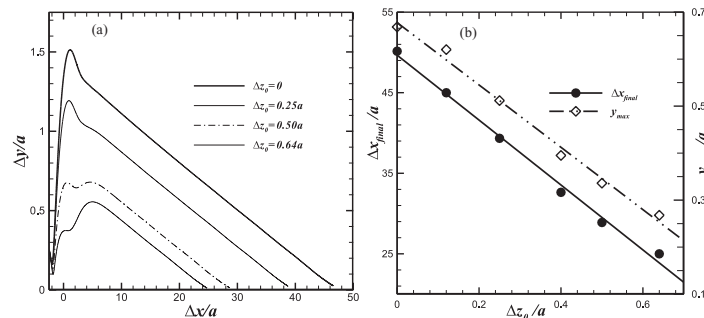


FIG. 4. (a) Effects of the initial separation in vorticity direction on the relative trajectory of a pair of drops at  $\Delta x_0/a = 2.5$ ,  $\Delta y_0/a = 0.25$ ,  $Ca = 0.20$ , and  $L_y = 5a$ . (b) Effects of  $\Delta z_0/a$  on  $\Delta x_{final}/a$  and  $y_{max}/a$ .

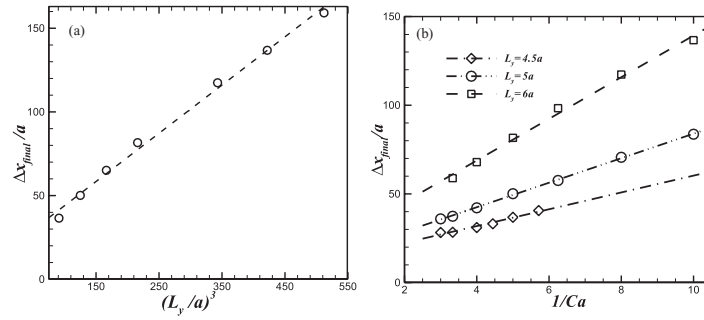


FIG. 5. (a) Effects of confinement in the gradient direction ( $L_y$ ) on  $\Delta x_{final}$  at  $Ca = 0.20$ . (b)  $\Delta x_{final}$  increases linearly with  $1/Ca$ .

shows  $u_y \sim -y (a/L_y)^3$ . Figure 7 similarly shows a scaling  $u_y \sim Ca$ . Therefore,

$$\frac{u_y}{\dot{\gamma}a} = -A \times Ca \left( \frac{a}{L_y} \right)^3 \left( \frac{y}{a} \right) \triangleq -\alpha \left( \frac{y}{a} \right), \quad A \text{ is a constant.} \quad (2)$$

Noting the symmetry between the top and the bottom drops (i.e.,  $\Delta y$  is twice the vertical separation of one of them from the centerline), one can integrate (2) to obtain

$$\frac{\Delta y}{a} = 2 \frac{y_{max}}{a} e^{-\alpha t \dot{\gamma}}. \quad (3)$$

Here  $\pm y_{max}$  are the post-collision vertical positions of the top and the bottom drops (measured from the centerline) wherefrom they follow a linear trajectory (Figure 2(b)). Then noting

$$\frac{dx}{dt} = \dot{\gamma} y = \dot{\gamma} y_{max} e^{-\alpha t \dot{\gamma}} \quad (4)$$

and the symmetry obtain

$$\frac{\Delta x}{a} = \frac{\Delta x_b}{a} + \frac{2}{\alpha} \left( \frac{y_{max}}{a} \right) (1 - e^{-\alpha t \dot{\gamma}}) = \frac{\Delta x_b}{a} + \frac{2}{\alpha} \left( \frac{y_{max}}{a} \right) - \frac{\Delta y}{\alpha a}, \quad (5)$$

where  $\Delta x_b$  is the flow wise separation immediately after collision. From Figure 2, it seems reasonable to assume that  $y_{max}$  and  $\Delta x_b$  are approximately independent of  $L_y$  and  $Ca$ . The relation suggested by (5) is verified by the collapse of relative trajectories for different  $L_y$  and  $Ca$  while scaling  $\Delta x$  with  $Ca(a/L_y)^3$  in Figure 8(b). Equation (5) after putting  $\Delta y_{final}/a = 0$  gives rise to

$$\frac{\Delta x_{final}}{a} = \frac{\Delta x_b}{a} + \frac{2}{A \times Ca} \left( \frac{L_y}{a} \right)^3 \left( \frac{y_{max}}{a} \right), \quad (6)$$

explaining  $\Delta x_{final}/a \sim (L_y/a)^3/Ca$  noted in (1). Figure 8(a) shows this scaling for a number of different  $L_y/a$  and  $Ca$ . The dotted line is a linear fit with  $A = 22.53$  and  $\Delta x_b/a = 12.30$  for

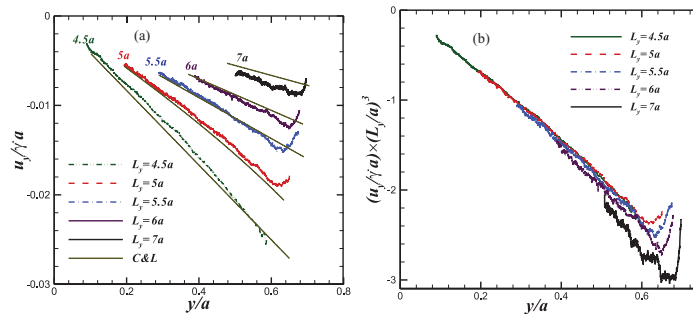


FIG. 6. (a) Variation of lateral velocity of the drops with  $y$  after collision with increasing confinement from the top at  $Ca = 0.20$  along with analytical results (straight lines) of Chan and Leal.<sup>31</sup> (b) The scaling of velocity with  $L_y$ .

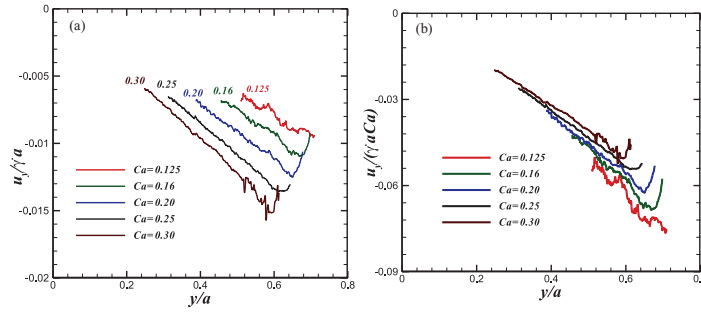


FIG. 7. (a) Variation of the post-collision lateral velocity of the drops with  $y$  at different  $Ca$  in the confined domain  $L_y = 6a$ . (b) The scaling of velocity with capillary numbers.

$y_{\max}/a = 0.67$ . The relation  $\Delta x_{\text{final}}/a \sim \Delta z_0/a$  seen in Figure 4(b) can be explained by noting that  $\Delta x_b/a$  is approximately invariant and  $y_{\max}$  varies linearly with  $\Delta z_0/a$  (Figure 4(b)).

Note that the relation (2) obtained from the numerically simulated velocities shown in Figures 6 and 7 proves critical to explain the observed scalings of  $\Delta x_{\text{final}}$ . To understand (2), we again note that the drop trajectories are straight lines after collision, indicating that the interactions between the drops then become negligible. Chan and Leal<sup>31</sup> performed a perturbative analysis of a single drop migrating in a shear plane between two parallel plates to get the following migration velocity:

$$\frac{u_y}{\dot{\gamma}a} = \frac{16 + 19\lambda}{16 + 16\lambda} \frac{3(54 + 97\lambda + 54\lambda^2)}{70(1 + \lambda)^2} Ca \left( \frac{a}{L_y} \right)^3 \left( -y^* - \frac{8y^*}{\left(1 - 4\left(\frac{ay^*}{L_y}\right)^2\right)^2} \right), \quad (7)$$

where  $y^* = y/a$ . For small  $y^*$  it can be linearized to obtain Eq. (2) with  $A = 21.62$  for  $\lambda = 1$ , which is sufficiently close to the linear fit ( $A = 22.53$ ) of  $\Delta x_{\text{final}}/a$  in Figure 8(a). Also the simulated velocity matches surprisingly well with this relation (shown by the straight lines) in Figure 6(a) for different  $L_y/a$ . Figure 9 shows the effects of viscosity ratio  $\lambda \neq 1$ . We note in the limit  $\lambda \rightarrow \infty$  the case reduces to a rigid sphere considered previously<sup>24</sup> which would lead to particles reaching free streamlines. Therefore, as expected, with increasing viscosity ratio,  $\Delta x_{\text{final}}/a$  increases. Figure 9 indicates that  $\lambda$  affects strongly  $y_{\max}$  and slightly  $\Delta x_b$ . The Chan and Leal expression(7) does not match the simulated migration velocity for  $\lambda$  much larger than unity. The result (6) can be rewritten including the  $\lambda$  dependence of migration velocity by a function  $g(\lambda)$ :

$$\frac{\Delta x_{\text{final}}}{a} = \frac{\Delta x_b}{a} + \frac{g(\lambda)}{Ca} \left( \frac{L_y}{a} \right)^3 \left( \frac{y_{\max}(\lambda)}{a} \right).$$

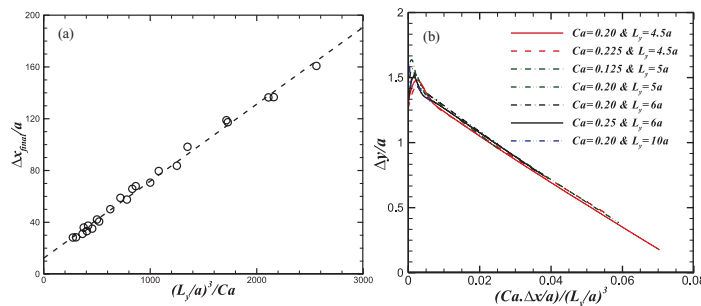


FIG. 8. (a) Composite scaling of  $\Delta x_{\text{final}}/a$  with  $L_y$  and  $Ca$  for many different values of  $L_y$  and  $Ca$ . (b) The relative trajectory of the drops with appropriate scaling.

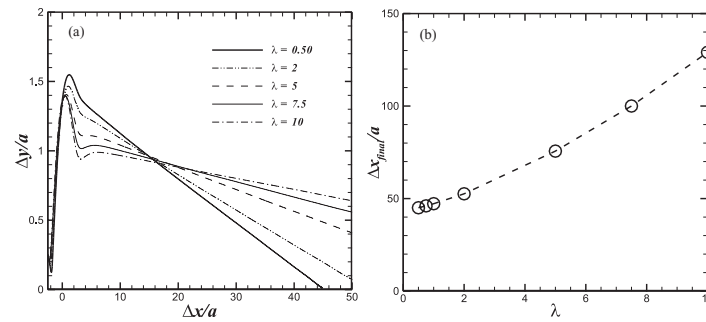


FIG. 9. (a) Effects of  $\lambda$  on the relative trajectory of a pair of drops at  $\Delta x_0/a = 2.5$ ,  $\Delta y_0/a = 0.25$ ,  $\Delta z_0/a = 0$ ,  $Ca = 0.20$ , and  $L_y = 5a$ . (b) The effect of  $\lambda$  on  $\Delta x_{final}/a$ .

Drops achieving a finite separation ( $\Delta x_{final}/a$ ) in the flow direction in a confined shear is a novel physical phenomenon and to our knowledge has not been mentioned in the literature before. It is analogous to others where particulate system organizes into specific spatial ordering.<sup>32</sup> However, here it is mediated exclusively by hydrodynamic interactions. Note that recently a particle based simulation of small number (3 and 6) of red blood cells (RBC) in extremely small capillaries (radius 1.23–1.75 times the effective radius of RBCs) showed them forming clusters in the middle of the capillaries. As here, RBC deformation caused their migration away from the wall. However, note that RBCs in that study were modeled as biconcave vesicles encapsulated by a complex elastic membrane that assumes the shape of a parachute at high flow rate, mediating the hydrodynamics of clustering phenomenon.<sup>33</sup> Although we chose to simulate a symmetric geometry with both walls moving in opposite directions, with a change of reference frame the physics (relative trajectory of particles) remains identical for the case, when one wall moves and the other remains stationary. (It was numerically verified but results are not shown.) The phenomenon reported here assumes further importance in view of the independence of the final separation of the initial drop positions when the drops are in the same shear plane (the separation varies linearly with separation in the vorticity direction). It indicates that a dilute emulsion of drops in a confined shear would have a tendency to organize into a single file separated by a specific distance that would depend on intrinsic hydrodynamic parameters, viz., capillary number and degree of confinement. Note that the parameters studied here are realizable in microfluidic devices. In a 10  $\mu\text{m}$  channel a velocity of 1 cm/s produces a shear rate  $\dot{\gamma} \sim 10^3 \text{ s}^{-1}$ ; with  $\mu \sim 1\text{--}100$  mN/m (water viscosity 1 mN/m),  $\Gamma \sim 1\text{--}100$  mN/m, for a 2  $\mu\text{m}$  drop ( $L_y/a = 5$ ) capillary number is  $Ca \sim 0.00002\text{--}0.2$  also obtained in microfluidic devices.<sup>1,34</sup> We have investigated drop interactions in linear shear instead of in a pressure driven flow—more often used in such devices—because the linear shear separates the shear effects on migration from those due to shear gradient present in a pressure driven flow. The present phenomenon of spatial ordering can be interrogated, e.g., optically, as a means for determining either size or deformability, both parameters affect capillary number. Differential migration also offers a way of filtering based on the same parameters. There has been a recent surge in innovative applications of size-differentiated inertial migration of rigid particles in pressure driven microfluidic devices for developing sorting, focusing, and flow cytometry.<sup>35–38</sup> Deformation provides an additional parameter to control migration and in systems with inertia will create additional migratory effects. Linear chain of droplets separated by a fixed distance has recently seen many novel applications such as determination of the time evolution of reaction kinetics, protein crystallization, and concentration indexing using specially designed droplet-pairs.<sup>39–41</sup>

<sup>1</sup> H. A. Stone, A. D. Stroock, and A. Ajdari, “Engineering flows in small devices: Microfluidics toward a lab-on-a-chip,” *Ann. Rev. Fluid Mech.* **36**, 381–411 (2004).

<sup>2</sup> O. A. Basaran, “Small-scale free surface flows with breakup: Drop formation and emerging applications,” *AIChE J.* **48**(9), 1842–1848 (2002).

<sup>3</sup> T. M. Squires and S. R. Quake, “Microfluidics: Fluid physics at the nanoliter scale,” *Rev. Mod. Phys.* **77**(3), 977–1026 (2005).

<sup>4</sup> S. Y. Teh, R. Lin, L. H. Hung, and A. P. Lee, “Droplet microfluidics,” *Lab Chip* **8**(2), 198–220 (2008).

<sup>5</sup> R. Skalak, N. Ozkaya, and T. C. Skalak, “Biofluid mechanics,” *Annu. Rev. Fluid Mech.* **21**, 167–204 (1989).

- <sup>6</sup> L. G. Leal, *Advanced Transport Phenomena: Fluid Mechanics and Convective Transport Processes* (Cambridge University Press, Cambridge, 2007).
- <sup>7</sup> F. P. Bretherton, "The motion of rigid particles in a shear flow at low Reynolds number," *J. Fluid Mech.* **14**(2), 284–304 (1962).
- <sup>8</sup> C. E. Chaffey, H. Brenner, and S. G. Mason, "Particle motions in sheared suspensions XVIII: Wall migration," *Rheol. Acta* **4**(1), 64 (1965).
- <sup>9</sup> A. Karnis and S. G. Mason, "Particle motions in sheared suspensions: XXIII. Wall migration of fluid drops," *J. Colloid Interface Sci.* **24**(2), 164 (1967).
- <sup>10</sup> S. Guido and M. Simeone, "Binary collision of drops in simple shear flow by computer-assisted video optical microscopy," *J. Fluid Mech.* **357**, 1–20 (1998).
- <sup>11</sup> M. Loewenberg and E. J. Hinch, "Collision of two deformable drops in shear flow," *J. Fluid Mech.* **338**, 299–315 (1997).
- <sup>12</sup> P. O. Olapade, R. K. Singh, and K. Sarkar, "Pair-wise interactions between deformable drops in free shear at finite inertia," *Phys. Fluids* **21**, 063302 (2009).
- <sup>13</sup> R. K. Singh and K. Sarkar, "Effects of viscosity ratio and three dimensional positioning on hydrodynamic interactions between two viscous drops in a shear flow at finite inertia," *Phys. Fluids* **21**(10), 103303 (2009).
- <sup>14</sup> G. Segre and A. Silberberg, "Radial particle displacements in Poiseuille flow of suspensions," *Nature (London)* **189**(476), 209–210 (1961).
- <sup>15</sup> A. Karnis, H. L. Goldsmit, and S. G. Mason, "Flow of suspensions through tubes. V. Inertial effects," *Can. J. Chem. Eng.* **44**(4), 181–193 (1966).
- <sup>16</sup> R. C. Jeffrey and J. R. A. Pearson, "Particle motion in laminar vertical tube flow," *J. Fluid Mech.* **22**, 721–735 (1965).
- <sup>17</sup> P. G. Saffman, "Lift on a small sphere in a slow shear flow," *J. Fluid Mech.* **22**, 385–400 (1965).
- <sup>18</sup> B. P. Ho and L. G. Leal, "Inertial migration of rigid spheres in two-dimensional unidirectional flows," *J. Fluid Mech.* **65**, 365–400 (1974).
- <sup>19</sup> P. Vasseur and R. G. Cox, "Lateral migration of a spherical-particle in two-dimensional shear flows," *J. Fluid Mech.* **78**, 385–413 (1976).
- <sup>20</sup> J. P. Matas, J. F. Morris, and E. Guazzelli, "Lateral forces on a sphere," *Oil Gas Sci. Technol.* **59**(1), 59–70 (2004).
- <sup>21</sup> P. M. Kulkarni and J. F. Morris, "Pair-sphere trajectories in finite-Reynolds-number shear flow," *J. Fluid Mech.* **596**, 413–435 (2008).
- <sup>22</sup> D. R. Mikulencak and J. F. Morris, "Stationary shear flow around fixed and free bodies at finite Reynolds number," *J. Fluid Mech.* **520**, 215–242 (2004).
- <sup>23</sup> G. Subramanian and D. L. Koch, "Centrifugal forces alter streamline topology and greatly enhance the rate of heat and mass transfer from neutrally buoyant particles to a shear flow," *Phys. Rev. Lett.* **96**(13), 134503 (2006).
- <sup>24</sup> M. Zurita-Gotor, J. Blawdziewicz, and E. Wajnryb, "Swapping trajectories: A new wall-induced cross-streamline particle migration mechanism in a dilute suspension of spheres," *J. Fluid Mech.* **592**, 447–469 (2007).
- <sup>25</sup> I. E. Zarraga and D. T. Leighton, "Measurement of an unexpectedly large shear-induced self-diffusivity in a dilute suspension of spheres," *Phys. Fluids* **14**(7), 2194–2201 (2002).
- <sup>26</sup> G. Tryggvason, B. Bunner, A. Esmaeeli, D. Juric, N. Al-Rawahi, W. Tauber, J. Han, S. Nas, and Y. J. Jan, "A front-tracking method for the computations of multiphase flow," *J. Comput. Phys.* **169**(2), 708–759 (2001).
- <sup>27</sup> K. Sarkar and W. R. Schowalter, "Deformation of a two-dimensional drop at non-zero Reynolds number in time-periodic extensional flows: Numerical simulation," *J. Fluid Mech.* **436**, 177–206 (2001).
- <sup>28</sup> X. Y. Li and K. Sarkar, "Drop dynamics in an oscillating extensional flow at finite Reynolds numbers," *Phys. Fluids* **17**(2), 027103 (2005).
- <sup>29</sup> X. Y. Li and K. Sarkar, "Drop deformation and breakup in a vortex at finite inertia," *J. Fluid Mech.* **564**, 1–23 (2006).
- <sup>30</sup> V. Sibillo, G. Pasquariello, M. Simeone, V. Cristini, and S. Guido, "Drop deformation in microconfined shear flow," *Phys. Rev. Lett.* **97**(5), 054502 (2006).
- <sup>31</sup> P. C.-H. Chan and L. G. Leal, "The motion of a deformable drop in a second-order fluid," *J. Fluid Mech.* **92**(1), 131–170 (1979).
- <sup>32</sup> M. Baron, J. Blawdziewicz, and E. Wajnryb, "Hydrodynamic crystals: Collective dynamics of regular arrays of spherical particles in a parallel-wall channel," *Phys. Rev. Lett.* **100**(17), 174502 (2008).
- <sup>33</sup> J. L. McWhirter, H. Noguchi, and G. Gompper, "Deformation and clustering of red blood cells in microcapillary flows," *Soft Matter* **7**(22), 10967–10977 (2011).
- <sup>34</sup> D. R. Link, S. L. Anna, D. A. Weitz, and H. A. Stone, "Geometrically mediated breakup of drops in microfluidic devices," *Phys. Rev. Lett.* **92**(5), 054503 (2004).
- <sup>35</sup> D. Di Carlo, D. Irimia, R. G. Tompkins, and M. Toner, "Continuous inertial focusing, ordering, and separation of particles in microchannels," *Proc. Natl. Acad. Sci. U.S.A.* **104**(48), 18892–18897 (2007).
- <sup>36</sup> D. Di Carlo, "Inertial microfluidics," *Lab Chip* **9**(21), 3038–3046 (2009).
- <sup>37</sup> A. A. S. Bhagat, S. S. Kuntaegowdanahalli, and I. Papautsky, "Enhanced particle filtration in straight microchannels using shear-modulated inertial migration," *Phys. Fluids* **20**(10), 101702 (2008).
- <sup>38</sup> A. A. S. Bhagat, S. S. Kuntaegowdanahalli, and I. Papautsky, "Inertial microfluidics for continuous particle filtration and extraction," *Microfluid. Nanofluid.* **7**(2), 217–226 (2009).
- <sup>39</sup> H. Song and R. F. Ismagilov, "Millisecond kinetics on a microfluidic chip using nanoliters of reagents," *J. Am. Chem. Soc.* **125**(47), 14613–14619 (2003).
- <sup>40</sup> H. Song, J. D. Tice, and R. F. Ismagilov, "A microfluidic system for controlling reaction networks in time," *Angew. Chem. Int., Ed.* **42**(7), 768–772 (2003).
- <sup>41</sup> B. Zheng, J. D. Tice, L. S. Roach, and R. F. Ismagilov, "A droplet-based, composite PDMS/glass capillary microfluidic system for evaluating protein crystallization conditions by microbatch and vapor-diffusion methods with on-chip X-ray diffraction," *Angew. Chem. Int. Ed.* **43**(19), 2508–2511 (2004).